Supplemental Material for *Toward better understanding of the high-pressure structural transformation in beryllium by the statistical moment method*

Tran Dinh Cuong[1,*] and Anh D. Phan[1,2]

[1] *Faculty of Materials Science and Engineering, Phenikaa University, Hanoi 12116, Vietnam.*
[2] *Phenikaa Institute for Advanced Study (PIAS), Phenikaa University, Hanoi 12116, Vietnam.*

I. VIBRATIONAL PARAMETERS OF BERYLLIUM

A. hcp Beryllium

The vibrational parameters of hcp beryllium are explicitly expressed by [S1, S2]

$$k = 2\frac{d^2\varphi_1}{dR_1^2} + \frac{4}{R_1}\frac{d\varphi_1}{dR_1} + \frac{1}{2}\frac{d^2\varphi_2}{dR_1^2} + \frac{1}{R_1}\frac{d\varphi_2}{dR_1} + \frac{3}{8R_1}\frac{d\varphi_3}{dR_1} + \frac{23}{18}\frac{d^2\varphi_4}{dR_1^2} + \frac{31}{18R_1}\frac{d\varphi_4}{dR_1}, \tag{S1}$$

$$\begin{aligned}\beta = {} & 0.144338\frac{d^3\varphi_1}{dR_1^3} - \frac{0.433013}{R_1}\frac{d^2\varphi_1}{dR_1^2} + \frac{0.433013}{R_1^2}\frac{d\varphi_1}{dR_1} - 0.144338\frac{d^3\varphi_2}{dR_1^3} + \frac{0.433013}{R_1}\frac{d^2\varphi_2}{dR_1^2} - \frac{0.433013}{R_1^2}\frac{d\varphi_2}{dR_1} \\ & + 0.106917\frac{d^3\varphi_4}{dR_1^3} - \frac{0.32075}{R_1}\frac{d^2\varphi_4}{dR_1^2} + \frac{0.32075}{R_1^2}\frac{d\varphi_4}{dR_1},\end{aligned} \tag{S2}$$

$$\begin{aligned}\gamma_1 = {} & \frac{5}{96}\frac{d^4\varphi_1}{dR_1^4} + \frac{3}{16R_1}\frac{d^3\varphi_1}{dR_1^3} + \frac{1}{32R_1^2}\frac{d^2\varphi_1}{dR_1^2} - \frac{1}{32R_1^3}\frac{d\varphi_1}{dR_1} + \frac{1}{192}\frac{d^4\varphi_2}{dR_1^4} + \frac{1}{32R_1}\frac{d^3\varphi_2}{dR_1^3} - \frac{1}{64R_1^2}\frac{d^2\varphi_2}{dR_1^2} + \frac{1}{64R_1^3}\frac{d\varphi_2}{dR_1} \\ & + \frac{9}{512R_1^2}\frac{d^2\varphi_3}{dR_1^2} - \frac{9}{512R_1^3}\frac{d\varphi_3}{dR_1} + \frac{179}{15552}\frac{d^4\varphi_4}{dR_1^4} + \frac{97}{2592R_1}\frac{d^3\varphi_4}{dR_1^3} - \frac{113}{5184R_1^2}\frac{d^2\varphi_4}{dR_1^2} + \frac{113}{5184R_1^3}\frac{d\varphi_4}{dR_1},\end{aligned} \tag{S3}$$

$$\begin{aligned}\gamma_2 = {} & \frac{5}{48}\frac{d^4\varphi_1}{dR_1^4} + \frac{3}{8R_1}\frac{d^3\varphi_1}{dR_1^3} + \frac{1}{16R_1^2}\frac{d^2\varphi_1}{dR_1^2} - \frac{1}{16R_1^3}\frac{d\varphi_1}{dR_1} + \frac{1}{96}\frac{d^4\varphi_2}{dR_1^4} + \frac{1}{16R_1}\frac{d^3\varphi_2}{dR_1^3} - \frac{1}{32R_1^2}\frac{d^2\varphi_2}{dR_1^2} + \frac{1}{32R_1^3}\frac{d\varphi_2}{dR_1} \\ & + \frac{9}{256R_1^2}\frac{d^2\varphi_3}{dR_1^2} - \frac{9}{256R_1^3}\frac{d\varphi_3}{dR_1} + \frac{179}{7776}\frac{d^4\varphi_4}{dR_1^4} + \frac{97}{1296R_1}\frac{d^3\varphi_4}{dR_1^3} - \frac{113}{2592R_1^2}\frac{d^2\varphi_4}{dR_1^2} + \frac{113}{2592R_1^3}\frac{d\varphi_4}{dR_1}.\end{aligned} \tag{S4}$$

Here, we define

$$\varphi_1 = -b_1\left[1 + b_2\left(R_1 - b_3\right)\right]\exp\left[-b_2\left(R_1 - b_3\right)\right], \tag{S5}$$

$$\varphi_2 = -b_1\left[1 + b_2\left(R_1\sqrt{2} - b_3\right)\right]\exp\left[-b_2\left(R_1\sqrt{2} - b_3\right)\right], \tag{S6}$$

$$\varphi_3 = -b_1\left[1 + b_2\left(R_1\sqrt{\frac{8}{3}} - b_3\right)\right]\exp\left[-b_2\left(R_1\sqrt{\frac{8}{3}} - b_3\right)\right], \tag{S7}$$

$$\varphi_4 = -b_1\left[1 + b_2\left(R_1\sqrt{3} - b_3\right)\right]\exp\left[-b_2\left(R_1\sqrt{3} - b_3\right)\right]. \tag{S8}$$

Note that the nearest neighbor distance R_1 is linked to the atomic volume V via

$$R_1 = \left(V\sqrt{2}\right)^{\frac{1}{3}}. \tag{S9}$$

*Electronic address: cuong.trandinh@phenikaa-uni.edu.vn

B. bcc Beryllium

For bcc beryllium, we have [S1, S2]

$$k = \frac{4}{3}\frac{d^2\varphi_1}{dR_1^2} + \frac{8}{3R_1}\frac{d\varphi_1}{dR_1} + \frac{3}{4}\frac{d^2\varphi_2}{dR_1^2} + \frac{3}{2R_1}\frac{d\varphi_2}{dR_1} + \frac{3}{4}\frac{d^2\varphi_3}{dR_1^2} + \frac{3}{2R_1}\frac{d\varphi_3}{dR_1} + \frac{12}{11}\frac{d^2\varphi_4}{dR_1^2} + \frac{24}{11R_1}\frac{d\varphi_4}{dR_1} + \frac{1}{3}\frac{d^2\varphi_5}{dR_1^2} + \frac{2}{3R_1}\frac{d\varphi_5}{dR_1}, \tag{S10}$$

$$\beta = 0, \tag{S11}$$

$$\begin{aligned}\gamma_1 = {} & \frac{1}{54}\frac{d^4\varphi_1}{dR_1^4} + \frac{2}{9R_1}\frac{d^3\varphi_1}{dR_1^3} - \frac{2}{9R_1^2}\frac{d^2\varphi_1}{dR_1^2} + \frac{2}{9R_1^3}\frac{d\varphi_1}{dR_1} + \frac{3}{128}\frac{d^4\varphi_2}{dR_1^4} + \frac{9}{64R_1^2}\frac{d^2\varphi_2}{dR_1^2} - \frac{9}{64R_1^3}\frac{d\varphi_2}{dR_1} + \frac{3}{512}\frac{d^4\varphi_3}{dR_1^4} \\ & + \frac{9}{256R_1}\frac{d^3\varphi_3}{dR_1^3} - \frac{9}{512R_1^2}\frac{d^2\varphi_3}{dR_1^2} + \frac{9}{512R_1^3}\frac{d\varphi_3}{dR_1} + \frac{249}{29282}\frac{d^4\varphi_4}{dR_1^4} + \frac{342}{14641R_1}\frac{d^3\varphi_4}{dR_1^3} + \frac{234}{14641R_1^2}\frac{d^2\varphi_4}{dR_1^2} \\ & - \frac{234}{14641R_1^3}\frac{d\varphi_4}{dR_1} + \frac{1}{864}\frac{d^4\varphi_5}{dR_1^4} + \frac{1}{72R_1}\frac{d^3\varphi_5}{dR_1^3} - \frac{1}{72R_1^2}\frac{d^2\varphi_5}{dR_1^2} + \frac{1}{72R_1^3}\frac{d\varphi_5}{dR_1},\end{aligned} \tag{S12}$$

$$\begin{aligned}\gamma_2 = {} & \frac{1}{9}\frac{d^4\varphi_1}{dR_1^4} + \frac{2}{3R_1^2}\frac{d^2\varphi_1}{dR_1^2} - \frac{2}{3R_1^3}\frac{d\varphi_1}{dR_1} + \frac{9}{32R_1}\frac{d^3\varphi_2}{dR_1^3} - \frac{27}{64R_1^2}\frac{d^2\varphi_2}{dR_1^2} + \frac{27}{64R_1^3}\frac{d\varphi_2}{dR_1} + \frac{9}{512}\frac{d^4\varphi_3}{dR_1^4} + \frac{9}{256R_1}\frac{d^3\varphi_3}{dR_1^3} \\ & + \frac{27}{512R_1^2}\frac{d^2\varphi_3}{dR_1^2} - \frac{27}{512R_1^3}\frac{d\varphi_3}{dR_1} + \frac{171}{14641}\frac{d^4\varphi_4}{dR_1^4} + \frac{1152}{14641R_1}\frac{d^3\varphi_4}{dR_1^3} - \frac{702}{14641R_1^2}\frac{d^2\varphi_4}{dR_1^2} + \frac{702}{14641R_1^3}\frac{d\varphi_4}{dR_1} \\ & + \frac{1}{144}\frac{d^4\varphi_5}{dR_1^4} + \frac{1}{24R_1^2}\frac{d^2\varphi_5}{dR_1^2} - \frac{1}{24R_1^3}\frac{d\varphi_5}{dR_1}.\end{aligned} \tag{S13}$$

Here, φ_1, φ_2, φ_3, φ_4, and φ_5 are written by

$$\varphi_1 = -b_1\left[1 + b_2\left(R_1 - b_3\right)\right]\exp\left[-b_2\left(R_1 - b_3\right)\right], \tag{S14}$$

$$\varphi_2 = -b_1\left[1 + b_2\left(R_1\frac{2}{\sqrt{3}} - b_3\right)\right]\exp\left[-b_2\left(R_1\frac{2}{\sqrt{3}} - b_3\right)\right], \tag{S15}$$

$$\varphi_3 = -b_1\left[1 + b_2\left(R_1\sqrt{\frac{8}{3}} - b_3\right)\right]\exp\left[-b_2\left(R_1\sqrt{\frac{8}{3}} - b_3\right)\right], \tag{S16}$$

$$\varphi_4 = -b_1\left[1 + b_2\left(R_1\sqrt{\frac{11}{3}} - b_3\right)\right]\exp\left[-b_2\left(R_1\sqrt{\frac{11}{3}} - b_3\right)\right], \tag{S17}$$

$$\varphi_5 = -b_1\left[1 + b_2\left(2R_1 - b_3\right)\right]\exp\left[-b_2\left(2R_1 - b_3\right)\right]. \tag{S18}$$

The relation between the nearest neighbor distance R_1 and the atomic volume V in the bcc phase is

$$R_1 = \left(\frac{3\sqrt{3}}{4}V\right)^{\frac{1}{3}}. \tag{S19}$$

II. EFFECTIVENESS OF MODIFIED WHEP MODEL

Thanks to state-of-the-art DAC and SW techniques, physicists have come very close to the actual high-pressure melting curve of bcc tantalum [S3], hcp iron [S4], and B1 magnesium oxide [S5]. Accordingly, we utilize these systems

Material	Structure	Bonding	B_0 (GPa)	B_0'	$T_\mathrm{m}(0)$ (K)	Reference
Tantalum	bcc	Metallic	194	3.524	3293	[S6, S9]
Iron	hcp	Metallic	177.7	5.64	1608	[S7, S10]
Magnesium Oxide	B1	Ionic	162.5	4.1	3250	[S8, S11]

TABLE S1: Input data for the modified WHEP model in the case of bcc tantalum, hcp iron, and B1 magnesium oxide.

to demonstrate the quality of the modified WHEP model (Equation (23)). Their EOS parameters are extracted from cutting-edge ramp-wave experiments [S6−S8] to avoid the great uncertainty caused by long EOS extrapolations. Detailed information about B_0, B_0', and $T_\mathrm{m}(0)$ is presented in Table S1 [S6−S11].

Figure S1 shows our theoretical calculations for the melting properties of bcc tantalum, hcp iron, and B1 magnesium oxide. Even though the selected materials have different crystalline structures and interatomic interactions, Equation (23) still works remarkably well. Our melting lines pass through most high-quality experimental points within the acceptable error range [S12−S23]. In particular, the consistency between WHEP analyses and DAC/SW measurements [S16−S19] for iron is maintained up to 1000 GPa, far beyond the Murnaghan limit ($P_\mathrm{Mur} \sim 355$ GPa). Note that we only use a single reference melting point for each material to achieve the above concurrences. These results confirm the accuracy and flexibility of our modified WHEP model.

III. INVALIDITY OF THE LINDEMANN LAW AND THE BURAKOVSKY-PRESTON-SILBAR THEORY FOR BERYLLIUM

For decades, the high-pressure melting behaviors of metals have been investigated by applying the well-known Lindemann law [S24] and the Burakovsky-Preston-Silbar (BPS) theory [S25]. According to Lindemann's physical picture [S24], the melting process is associated with the vibrational instability of the solid phase via

$$\frac{\langle u_\delta^2 \rangle}{R_1^2} = \lambda_\mathrm{L}. \tag{S20}$$

Meanwhile, from the BPS point of view [S25], the melting transition is strongly promoted by the proliferation of dislocation defects as

$$\frac{\mu V}{T_\mathrm{m}} = \lambda_\mathrm{PBS}, \tag{S21}$$

where μ is the shear modulus. For a given metallic substance, the Lindemann parameter λ_L and the BPS parameter λ_BPS are supposed to be unchanged along the melting line [S24, S25].

Figure S2 shows our numerical results for λ_L and λ_BPS along the SMM-WHEP solid-liquid boundary of beryllium. It is conspicuous that these parameters cannot remain constant during compression. Whereas $\lambda_\mathrm{L}(P_\mathrm{m}, T_\mathrm{m})/\lambda_\mathrm{L}(0, T_\mathrm{m}(0))$ grows significantly to 2.63 at 500 GPa, $\lambda_\mathrm{BPS}(P_\mathrm{m}, T_\mathrm{m})/\lambda_\mathrm{BPS}(0, T_\mathrm{m}(0))$ decreases sharply to 0.37 at the same condition. These dramatic changes affirm that the Lindemann law [S24] and the BPS theory [S25] are inadequate to capture the melting characteristics of beryllium at the quantitative level. Our conclusion is in line with the newest DFT simulations of Wu *et al.* [S26].

[S1] G. Leibfried and W. Ludwig, *Solid State Phys.* **12**, 275 (1961).
[S2] T. D. Cuong and A. D. Phan, *Phys. Chem. Chem. Phys.* **24**, 4910 (2022).
[S3] T. D. Cuong and A. D. Phan, *Vacuum* **179**, 109444 (2020).
[S4] T. D. Cuong, N. Q. Hoc, N. D. Trung, N. T. Thao, and A. D. Phan, *Phys. Rev. B* **106**, 094103 (2022).
[S5] T. D. Cuong and A. D. Phan, *Vacuum* **189**, 110231 (2021).
[S6] J. R. Rygg, J. H. Eggert, A. E. Lazicki, F. Coppari, J. A. Hawreliak, D. G. Hicks, R. F. Smith, C. M. Sorce, T. M. Uphaus, B. Yaakobi, and G. W. Collins, *Rev. Sci. Instrum.* **83**, 113904 (2012).
[S7] R. F. Smith, D. E. Fratanduono, D. G. Braun, T. S. Duffy, J. K. Wicks, P. M. Celliers, S. J. Ali, A. Fernandez-Panella, R. G. Kraus, D. C. Swift, G. W. Collins, and J. H. Eggert, *Nat. Astron.* **2**, 452 (2018).
[S8] F. Coppari, R. F. Smith, J. H. Eggert, J. Wang, J. R. Rygg, A. Lazicki, J. A. Hawreliak, G. W. Collins, and T. S Duffy, *Nat. Geosci.* **6**, 926 (2013).
[S9] J. F. Smith and O. N. Carlson, *Bull. Alloy Phase Diagr.* **4**, 284 (1983).
[S10] Y. Ma, M. Somayazulu, G. Shen, H. K. Mao, J. Shu, and R. J. Hemley, *Phys. Earth Planet. Inter.* **143**, 455 (2004).

[S11] C. Ronchi and M. Sheindlin, *J. Appl. Phys.* **90**, 3325 (2001).
[S12] A. Dewaele, M. Mezouar, N. Guignot, and P. Loubeyre, *Phys. Rev. Lett.* **104**, 255701 (2010).
[S13] C. Dai, J. Hu, and H. Tan, *J. Appl. Phys.* **106**, 043519 (2009).
[S14] J. Li, X. Zhou, J. Li, Q. Wu, L. Cai, and C. Dai, *Rev. Sci. Instrum.* **83**, 053902 (2012).
[S15] R. G. Kraus, F. Coppari, D. E. Fratanduono, R. F. Smith, A. Lazicki, C. Wehrenberg, J. H. Eggert, J. R. Rygg, and G. W. Collins, *Phys. Rev. Lett.* **126**, 255701 (2021).
[S16] S. Anzellini, A. Dewaele, M. Mezouar, P. Loubeyre, and G. Morard, *Science* **340**, 464 (2013).
[S17] M. Hou, J. Liu, Y. Zhang, X. Du, H. Dong, L. Yan, J. Wang, L. Wang, and B. Chen, *Geophys. Res. Lett.* **48**, e2021GL095739 (2021).
[S18] J. Li, Q. Wu, J. Li, T. Xue, Y. Tan, X. Zhou, Y. Zhang, Z. Xiong, Z. Gao, and T. Sekine, *Geophys. Res. Lett.* **47**, e2020GL087758 (2020).
[S19] R. G. Kraus, R. J. Hemley, S. J. Ali, J. L. Belof, L. X. Benedict, J. Bernier, D. Braun, R. E. Cohen, G. W. Collins, F. Coppari, M. P. Desjarlais, D. Fratanduono, S. Hamel, A. Krygier, A. Lazicki, J. Mcnaney, M. Millot, P. C. Myint, M. G. Newman, J. R. Rygg, D. M. Sterbentz, S. T. Stewart, L. Stixrude, D. C. Swift, C. Wehrenberg, and J. H. Eggert, *Science* **375**, 202 (2022).
[S20] Z. Du and K. K. M. Lee, *Geophys. Res. Lett.* **41**, 8061 (2014).
[S21] T. Kimura, H. Ohfuji, M. Nishi, and T. Irifune, *Nat. Commun.* **8**, 15735 (2017).
[S22] S. Fu, J. Yang, Y. Zhang, J. Liu, E. Greenberg, V. B. Prakapenka, T. Okuchi, and J. F. Lin, *Earth Planet. Sci. Lett.* **503**, 1 (2018).
[S23] O. V. Fat'yanov, P. D. Asimow, and T. J. Ahrens, *Phys. Rev. B* **97**, 024106 (2018).
[S24] F. A. Lindemann, *Phys. Z.* **11**, 609 (1910).
[S25] L. Burakovsky, D. L. Preston, and R. R. Silbar, *J. Appl. Phys.* **88**, 6294 (2000).
[S26] J. Wu, F. González-Cataldo, F. Soubiran, and B. Militzer, *J. Phys.: Condens. Matter* **34**, 144003 (2022).

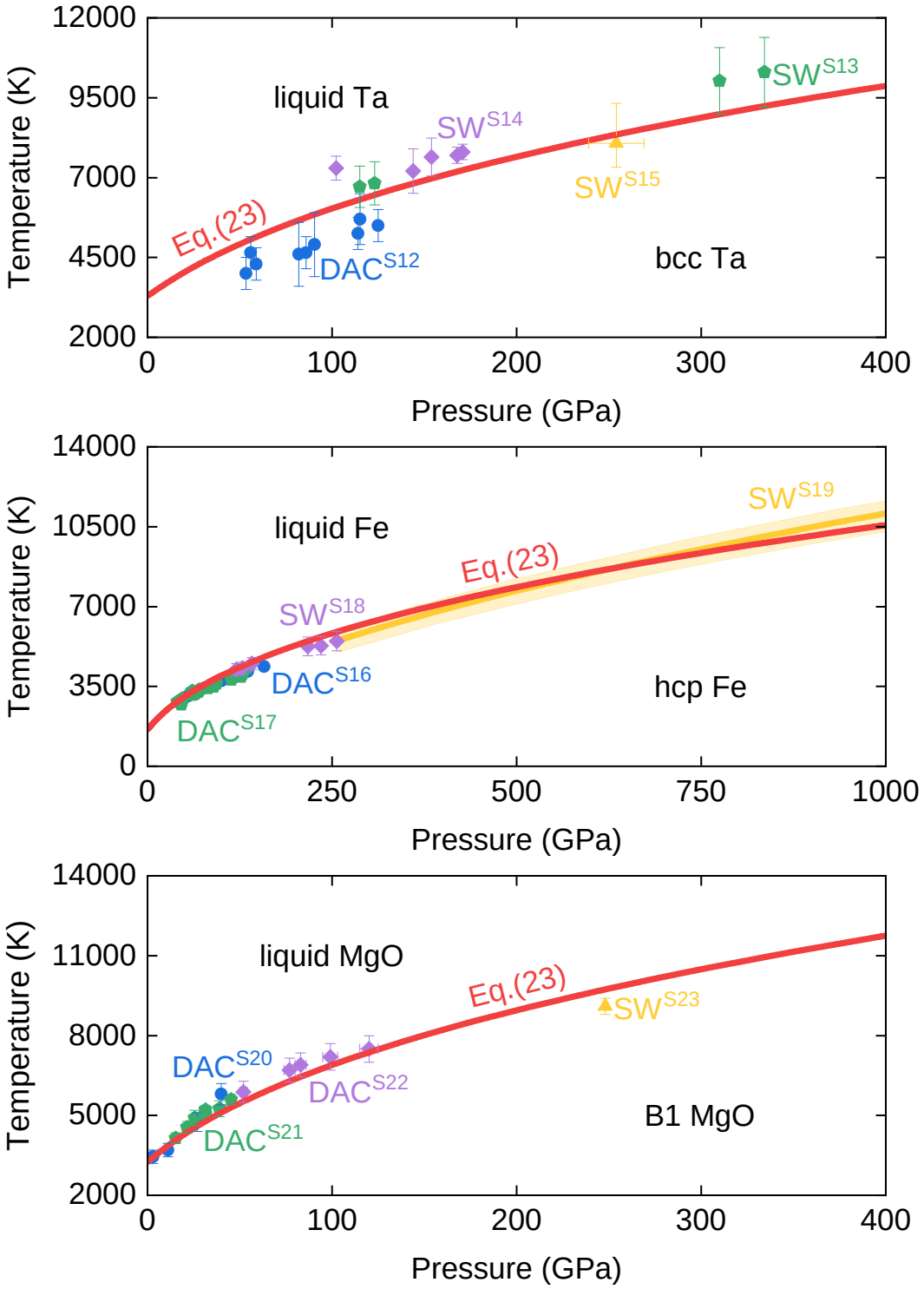

FIG. S1: (Color online) The melting boundary of bcc tantalum, hcp iron, and B1 magnesium oxide determined by our WHEP calculations and recent DAC/SW experiments [S12−S23].

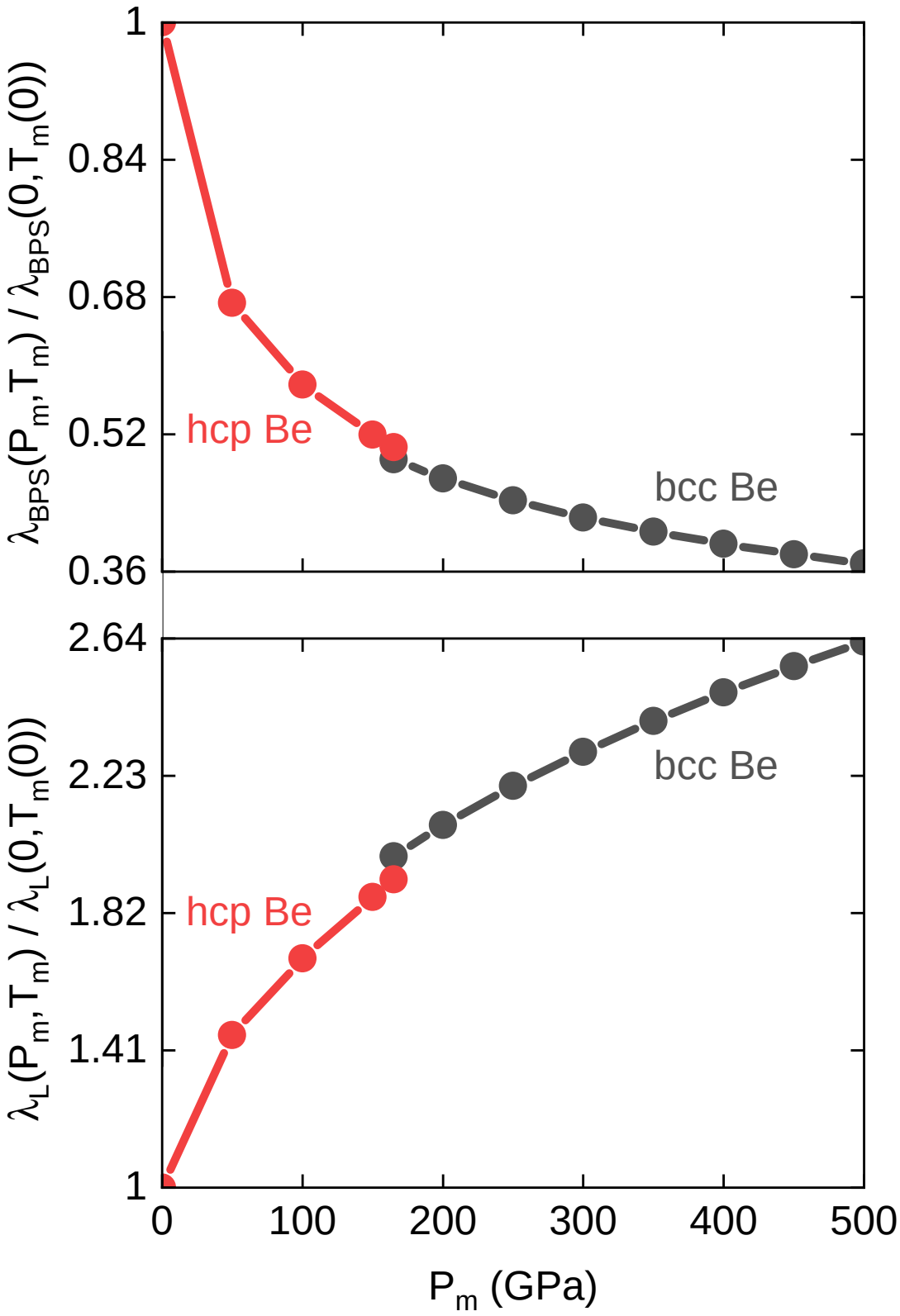

FIG. S2: (Color online) The variation of Lindemann and BPS parameters along the SMM-WHEP melting curve of beryllium.